Article

Determination of Initial-Shear-Stress Impact on Ramsar-Sand Liquefaction Susceptibility through Monotonic Triaxial Testing

Mehrdad Nategh[1], Abdullah Ekinci[2], Anoosheh Iravanian[3]*, and Siavash Salamatpoor[4]

[1] Department of civil engineering, University College of Rouzbahan, Sari, 3994548179, Iran; mehr.nategh@gmail.com
[2] Civil Engineering Program, Middle East Technical University, Northern Cyprus Campus, Kalkanli, Guzelyurt, North Cyprus, via Mersin 10, Turkey; ekincia@metu.edu.tr
[3] Near East University, Civil Engineering Department, Lefkosa, 99138, Mersin 10, Turkey; anoosheh.iravanian@neu.edu.tr
[4] Department of civil engineering, University College of Rouzbahan, Sari, 3994548179, Iran; ssalamatpoor@yahoo.com

* Correspondence: ekincia@metu.edu.tr; Tel.: +90-542-888-1440

Abstract: Liquefaction risk assessment is critical for the safety and economics of structures. As the soil strata of Ramsar area in north Iran is mostly composed of poorly graded clean sand and the ground water table is found at shallow depths, it is highly susceptible to liquefaction. In this study, a series of isotropic and anisotropic consolidated undrained triaxial tests are performed on reconstituted specimens of Ramsar sand to identify the liquefaction potential of the area. The specimens are consolidated isotropically to simulate the level ground condition, and anisotropically to simulate the soil condition on a slope and/ or under a structure. The various states of soil behavior are studied by preparing specimens at different initial relative densities and applying different levels of effective stress. The critical state soil mechanics approach for identifying the liquefaction susceptibility is adopted and the observed phenomena are further explained in relation to the micro-mechanical behavior. As only four among the 27 conducted tests did not exhibit liquefactive behavior, Ramsar sand can be qualified as strongly susceptible to liquefaction. Furthermore, it is observed that the pore pressure ratio is a good indication of the liquefaction susceptibility

Keywords: Anisotropic Triaxial test; Initial shear stress; Pore water pressure ratio; Static liquefaction; Ramsar sand.

---

some 1. Introduction

Soil liquefaction is a phenomenon in which soil loses its bearing capacity and behaves like a liquid. After Marcuson [1], Youd et al. [2] defined liquefaction as "the act or process of transforming any substance into a liquid". This phenomenon can damage a broad range of constructions such as dams, roads, and embankments. The study of liquefaction to develop susceptibility assessment approaches can enable the construction of safer structures, saving money and lives. The Niigata earthquake (1964) accelerated intense research on liquefaction. Experimental work on static liquefaction was originally performed by Castro [3], and Castro and Poulos [4]. Their work on static liquefaction using a triaxial apparatus provided a better perception of the liquefaction mechanism and its controlling parameters. The application of initial shear stress during sample consolidation is a method for studying the treatment of anisotropically consolidated samples. Jafarian et al. [5] observed that this method plays a significant role in stimulating the liquefaction susceptibility of the soil condition on a slope subjected to high shear strain or under a structure that can tolerate high

Preprints (www.preprints.org) | NOT PEER-REVIEWED | Posted: 5 September 2020 doi:10.20944/preprints202009.0118.v1

shear stresses. Castro [3] performed several static tests on anisotropically and isotropically consolidated undrained samples and distinguished three different types of behavior for sands, as shown in Figure 1.

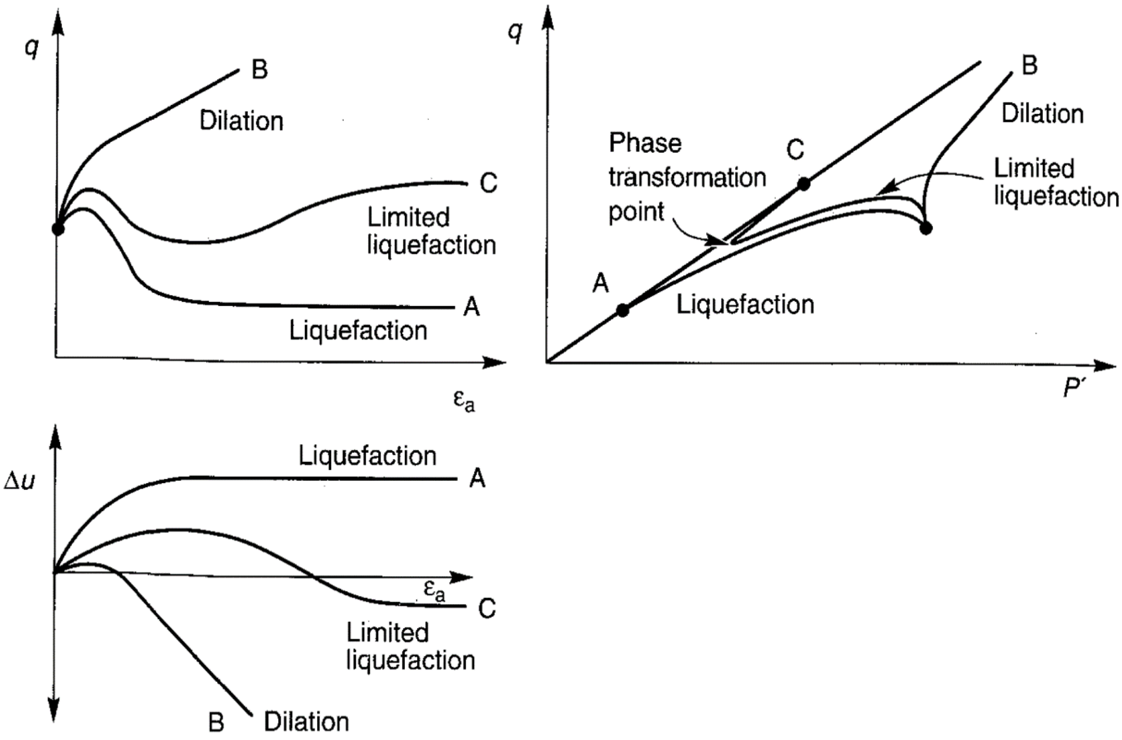

Figure 1. Liquefaction, limited liquefaction and dilation in static loading tests [3].

Numerous studies [4,6–12] have concluded that the initial state expressed in terms the initial void ratio e_0 as well as the initial effective mean stress p'_0 significantly affect undrained soil response. The influence of the initial shear stress on the liquefaction susceptibility has been investigated in recent decades. Kramer and Seed [13] observed that in samples consolidated to principal effective stress ratios (K`) of 1.5, 2.0, and 2.25, the increase in deviator stress under undrained conditions required to initiate liquefaction were approximately 0.6, 0.25, and 0.13 ksc (59, 25, and 13 kPa), respectively. They reported that the resistance to static liquefaction in these samples decreased significantly as the initial shear stress level increased. Later contributions by Harder and Boulanger [14], and Seed and Harder [15] demonstrated that the presence of the initial shear stress ratio improves liquefaction resistance at high relative densities (55–70%), whereas the effect is less pronounced at low relative densities (approximately 35%). According to recent research [16,17], triaxial tests performed at higher initial shear stress parameter values have a distinct effect for range of α. Alpha values could create both improving and aggravating effects on loose or very dense sands influence on the liquefaction susceptibility.

Soil samples under shearing up to large strains tend to reach a state of continuous deformation under constant shear (q) and normal stresses (p'), where such occurrence is known as the ultimate steady-state line (SSL). Soil at SSL exhibit a relationship between the ultimate values of the deviatoric stress and mean effective principal stress. Therefore, soil behavior can be predicted by expressing the state of the effective confining stress and defining the location of this point relative to the steady-state line. Castro and Poulos [4] observed that in addition to the steady-state line position being a unique soil property, the inclination of steady-state lines vary extensively, even for apparently similar soils. The steady-state concept and SSL were further described by other research [1,3,18]. Poulos et al. [4] systematically measured the steady strength through stress-controlled CU triaxial tests. On the other hand, Roscoe et al. [19] studied the yielding of soils and reported that when soil is subjected to shear distortion, it begins to shear at constant volume at a certain critical pressure. Similarly, according to

Preprints (www.preprints.org) | NOT PEER-REVIEWED | Posted: 5 September 2020 doi:10.20944/preprints202009.0118.v1

Schofield and Wroth [20], if a soil specimen is continuously distorted, it reaches steady state, i.e., flow failure. Although the critical state was initially developed on clayey soils, several studies have attempted to adopt this framework to granular materials [21,22]. However, Been et al. [23] stated that such an attempt is challenging due to the difficulties in determining the normal consolidation line for such soils. Coop [24] clarified that this phenomena involves stress formation at the particle contact points, affecting the compression response of granular materials. However, the attempts of Ferreira and Bica [25], Coop [26], Ekinci et al. [12], and Rezaian at al. [27] for adopting this framework to granular soils was successful.

To understand the critical state concept of granular materials, the microscale behavior of sandy soils was investigated. Cavarretta et. al. [28] studied the micromechanical behavior of coarse-grained soils utilizing a new technology to compute the particle shape and surface roughness, for measuring the particle contact stiffness and interparticle friction to relate the nature of fundamental particle behavior with the traditional test results (triaxial and oedometer). Although a link was established between the roughness of the particle surface and interparticle friction, the influence of the particle shape was more noticeable. In a similar study by Senetakis et al. [29], repeated interparticle shear testing showed a small decrease in the friction angle, which can be because of asperity damage during initial shearing. Recently, Zhang et. al. [30] investigated sands with a variety of minerology using shape analysis, particle crush tests, and one-dimensional compression tests. Authors reported that particle mineralogy could be a major factor affecting the strength or compressibility, rather than the particle shape. Moreover, Zhao et. al. [31] investigated the effect of the initial density of specimens in one-dimensional compression to evaluate particle breakage. They stated that specimens prepared with high relative density had lower probability of failure and failure modes that were less extensive compared to the low-density specimens. Moreover, it was reported that the effect of the initial density on the probability of particle survival reduced after significant breakage. Additionally, loose specimens exhibited higher compression due to particle failure leading to more fine generation by the further crushing of the existing fragments.

In support of the anisotropical soil condition on a slope and/ or under a structure, McDowell and Bolton [32] proved that compared to isotropic or k0 conditions, shearing was more effective at breaking particles. Furthermore, Coop et. al. [33] investigated particle breakage by performing ring shear tests and observed that particle breakage continued up to very large strains along with volumetric compression, which was observed even for tests at moderate confining stresses. Accordingly, Chandler [34] stated that the observed critical state at the strain levels reached by triaxial equipment was due to the counteracting dilative strains because of particle rearrangement and compressive strains because of particle breakage.

Liquefaction could be induced by static loading or cyclic loading. Fort Peck Dam and Nerlerk Berm failures are good examples for static liquefaction. Cyclic loading may take different forms like storm load, ice load and machinery load, on which Jefferies & Been [35] have given a good historical summary. The most tremendous one is, undoubtedly, that caused by earthquake shaking [36] in terms of the intensity of loading and extensity of damage triggered. The static loading concerned in this study is primarily in relation with monotonic loading occurs due to a sudden increase of pore water pressure and thus confining effective stress during an earthquake.

In this study, the effect of the initial shear stress ratio on the potential liquefaction susceptibility is investigated through monotonic testing. This study is the first to evaluate the liquefaction susceptibility by relating the pore pressure ratio (r_u) with the initial shear stress ratio (α) and explain the liquefaction phenomena in relation to the particle breakage mechanism. Furthermore, the adopted anisotropic testing mimics realistic scenarios such as the simulation of the soil condition on a slope and/or under a structure. Compared to level ground conditions (α = 0), only a few experimental studies on the monotonic behavior of sands in sloping ground conditions (α > 0) are available. Moreover, specimen testing in undrained triaxial condition reduces the testing time. Therefore, this study proposes a method for liquefaction susceptibility determination which is less time consuming, and less expensive than other widespread methods just like dynamic triaxial testing method.

Preprints (www.preprints.org) | NOT PEER-REVIEWED | Posted: 5 September 2020 doi:10.20944/preprints202009.0118.v1

2. Materials and Methods

2.1. Physical Parameters of Ramsar Sand

The relative density D_r is a critical parameter that can control the stress-strain behavior or change the liquefaction susceptibility. In this study, three values of the relative density (2%, 30%, and 45%) were considered to include very loose, loose, and medium dense sand, respectively. Ramsar sand is poorly graded clean sand which is extensively found in the southern coast of the Caspian Sea and classified as SP according to USCS. The e_{max} and e_{min} values of Ramsar sand, measured according to ASTM D-4253 [37], and ASTM D-4254 [38], are 0.88 and 0.54, respectively. The grain size distribution curve of Ramsar sand is depicted in Figure 2 and its basic properties are summarized in Table 1.

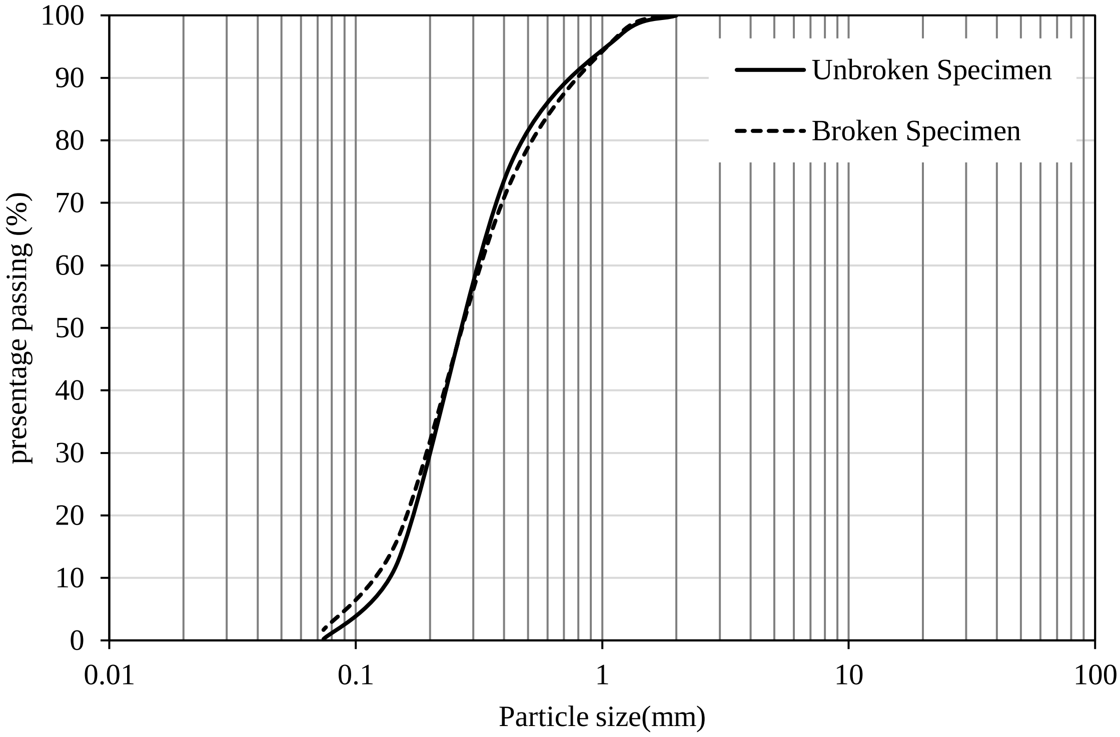

Figure 2. Grain size distribution for broken and unbroken Ramsar sand.

Table 1. Basic properties of Ramsar sand.

Parameters	Values
e_{max}	0.88
e_{min}	0.54
G_s	2.67
$D_{50}(mm)$	0.22
$D_{10}(mm)$	0.147
$D_{30}(mm)$	0.187
$D_{60}(mm)$	0.246
C_c	0.96

Preprints (www.preprints.org) | NOT PEER-REVIEWED | Posted: 5 September 2020 doi:10.20944/preprints202009.0118.v1

C_u	1.67

The grain size distribution of the specimens after triaxial testing were investigated and plotted against sand specimens obtained at 2-m depth from a borrow pit. Figure 2 shows that sand particles around 0.6–0.8 mm are further broken because there is a reduction in this particle percentage, whereas adversely, there is an increase in the particle percentage in the 0.1– 0.2 mm particle size range. This observation reveals that after shearing, Ramsar sand particles are brittle.

In order to further investigate this observation, sand particles before and after the test were examined using an optical microscope. The grains of the sand in Figure 3 (a) are rounded with certain sharp ends, whereas in Figure 3(b), the edges of the parent particle appear broken. Due to extensive shearing, more rounded particles are generated with very tiny spots related to broken bits of sand grains, clearly demonstrating the inherent brittleness. Moreover, the presence of silt is obvious in Figure 3.

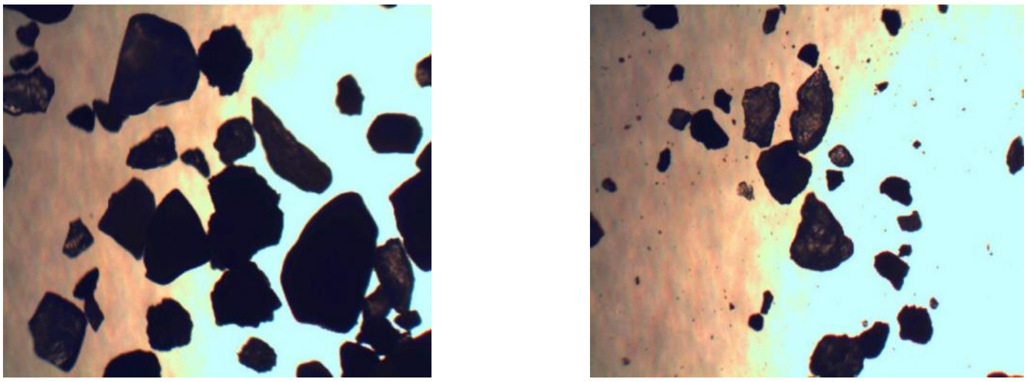

(**a**) (**b**)

Figure 3. Microscopic view (40x) of Ramsar sand, where (a) and (b) are respectively before and after the test.

Furthermore, in order to assess the influence of the observed phenomenon during undrained shearing, two tests under the same confining pressure and relative density (σ_{3c} = 350 kPa and Dr_0 = 30 %) were conducted on broken and unbroken sand. In these two tests, the ultimate deviatoric stress (q_u) for broken sand was higher (283.85 kPa) than that for the unbroken one (255.9 kPa), indicating that the former has more resistance to contractive behavior. Similar to these findings, Cavarretta et. al. [28] had reported that compared to the as supplied particles (perfectly rounded glass ballotini), crushed particles showed higher deviatoric stresses and more dilation.

2.2. Test Procedure

Moist tamping, which is the most common and valid method, was used to prepare the specimens. Sand specimens were oven-dried, mixed with 5% distilled water, and divided into five equal portions based on weight. Rubber membrane with a thickness of 0.3 mm was stretched by applying vacuum pressure. Each layer was then poured into a cylindrical split-mold, leveled with a spatula, and gently tamped. In order to improve the bonding between layers, the surface of each layer was scarified, and the same procedure was repeated for each layer. Measurement of the sample height and diameter was preceded by the application of a slight vacuum (not more than 20 kPa) on the specimen. The sample height and diameter were maintained at approximately 100 mm and 50 mm, respectively. Figure 4 illustrates a prepared sample. Subsequently, the cell was installed and filled with water. The vacuum was removed, and a positive pressure of approximately 30 kPa was applied. Carbon dioxide was infused through the specimen to augment saturation (to obtain a suitable degree of saturation, the carbon dioxide infusion technique proposed by Lade and Duncan [39] was used. Deaired water was then passed into soil under a specified back pressure to achieve

Preprints (www.preprints.org) | NOT PEER-REVIEWED | Posted: 5 September 2020 doi:10.20944/preprints202009.0118.v1

saturation of at least 95%. After consolidation, strain-controlled undrained loading (1 mm/ min) was applied and continued until the occurrence of specimen failure or 30-mm axial displacement. Anisotropic tests were conducted with a very-low-rate axial load applied to the sample in a drained condition.

(**a**) (**b**)

Figure 4. Examples of (a) preparation and (b) tested triaxial sample.

3. Results and Discussion

This study is primarily concerned with the effect of the initial shear stress on the potential susceptibility to the static liquefaction of Ramsar sand. It deals with specimens prepared at relative densities of 2%, 30%, and 45%. Isotropically (α=0) and anisotropically (α = 0.3 and 0.5) consolidated specimens under three different confining pressure (150, 250 and 350 kPa) were tested in an undrained condition. A brief explanation of all the 27 tests is presented in Table 2. In addition, all the stress path graphs are shown in Figure 5 (ACU and ICU denote anisotropically and isotropically consolidated undrained, respectively).

Preprints (www.preprints.org) | NOT PEER-REVIEWED | Posted: 5 September 2020 doi:10.20944/preprints202009.0118.v1

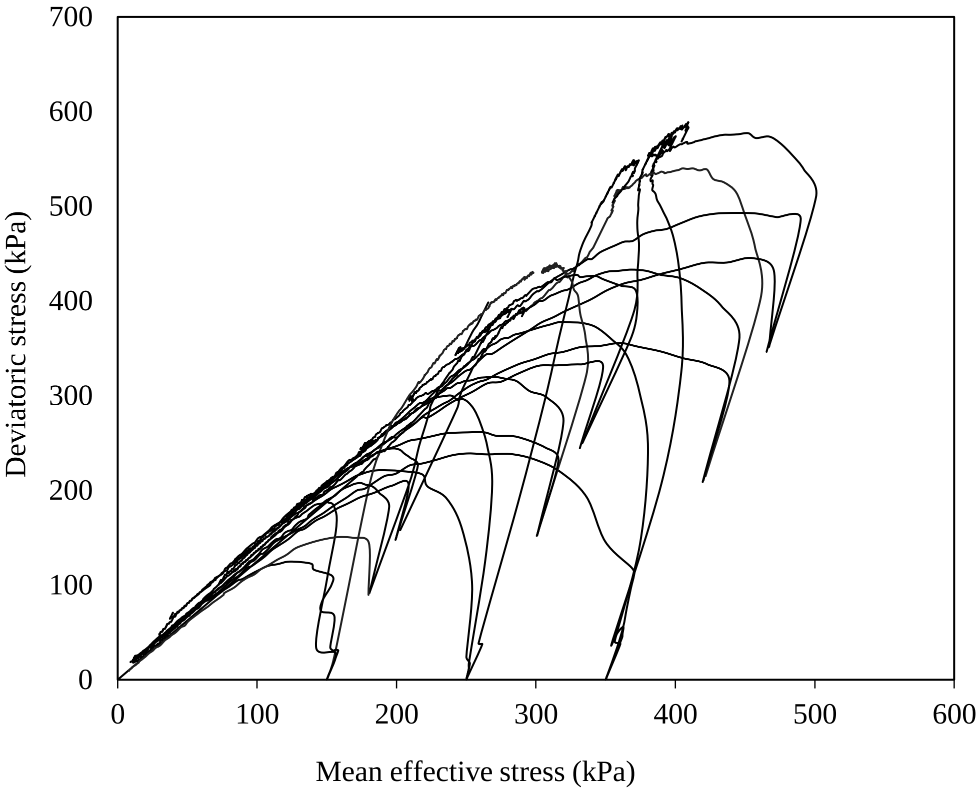

Figure 5. Steady state line in q-p′ plane with all 27 stress paths

Table 2. Summary of static triaxial tests conducted during the current study.

#	Series	α	Situ	σ_{3c}	D_{r0}	D_{rc}	Result
1	$(R\text{-}A)_1$	0	ICU	150	2	12.1	Liquefaction
2	$(R\text{-}A)_2$	0	ICU	150	30	37.5	Liquefaction
3	$(R\text{-}A)_3$	0	ICU	150	45	51.5	Dilation
4	$(R\text{-}A)_4$	0	ICU	250	2	16.6	Liquefaction
5	$(R\text{-}A)_5$	0	ICU	250	30	42.7	Liquefaction
6	$(R\text{-}A)_6$	0	ICU	250	45	53.77	Dilation
7	$(R\text{-}A)_7$	0	ICU	350	2	22.48	Liquefaction
8	$(R\text{-}A)_8$	0	ICU	350	30	37.37	Liquefaction
9	$(R\text{-}A)_9$	0	ICU	350	45	55.35	Limited
10	$(R\text{-}B)_1$	0.3	ACU	150	2	16.6	Liquefaction
11	$(R\text{-}B)_2$	0.3	ACU	150	30	38	Liquefaction
12	$(R\text{-}B)_3$	0.3	ACU	150	45	52.24	Dilation
13	$(R\text{-}B)_4$	0.3	ACU	250	2	20.6	Liquefaction
14	$(R\text{-}B)_5$	0.3	ACU	250	30	42.25	Liquefaction
15	$(R\text{-}B)_6$	0.3	ACU	250	45	54.3	Liquefaction

Preprints (www.preprints.org) | NOT PEER-REVIEWED | Posted: 5 September 2020 doi:10.20944/preprints202009.0118.v1

16	$(R\text{-}B)_7$	0.3	ACU	350	2	26.7	Liquefaction
17	$(R\text{-}B)_8$	0.3	ACU	350	30	44.91	Liquefaction
18	$(R\text{-}B)_9$	0.3	ACU	350	45	57.16	Liquefaction
19	$(R\text{-}C)_1$	0.5	ACU	150	2	18.55	Liquefaction
20	$(R\text{-}C)_2$	0.5	ACU	150	30	39.9	Liquefaction
2	$(R\text{-}C)_3$	0.5	ACU	150	45	53.02	Dilation
22	$(R\text{-}C)_4$	0.5	ACU	250	2	24.45	Liquefaction
23	$(R\text{-}C)_5$	0.5	ACU	250	30	43.7	Liquefaction
24	$(R\text{-}C)_6$	0.5	ACU	250	45	54.57	Limited
25	$(R\text{-}C)_7$	0.5	ACU	350	2	30.62	Liquefaction
26	$(R\text{-}C)_8$	0.5	ACU	350	30	41.94	Liquefaction
27	$(R\text{-}C)_9$	0.5	ACU	350	45	57.4	Liquefaction

The SSL for the 27 CU tests of Ramsar sand are displayed in Figure 6. The brittleness of the particles causes sample brakeage and fills in the available pores to bring the specimen to the same steady state as reported earlier by Cavarretta et al. [28]. Adversely, some researchers [12,40,41] had reported that poorly graded sand specimens prepared at varying relative densities had different SSLs. Ferreira and Bica [25], and Ekinci et al. [12] had tested a range of relative densities from minimum to maximum, and had managed to apply the critical state framework by grouping the relative densities and normalizing the results according to the group critical state line. Comparison of the relative densities of the specimens tested in this study with those of the study by Ekinci et al. [12] reveals that the densities of the specimens in this study falling into Group which is located at a position closest to the NCL, reach the same SSL.

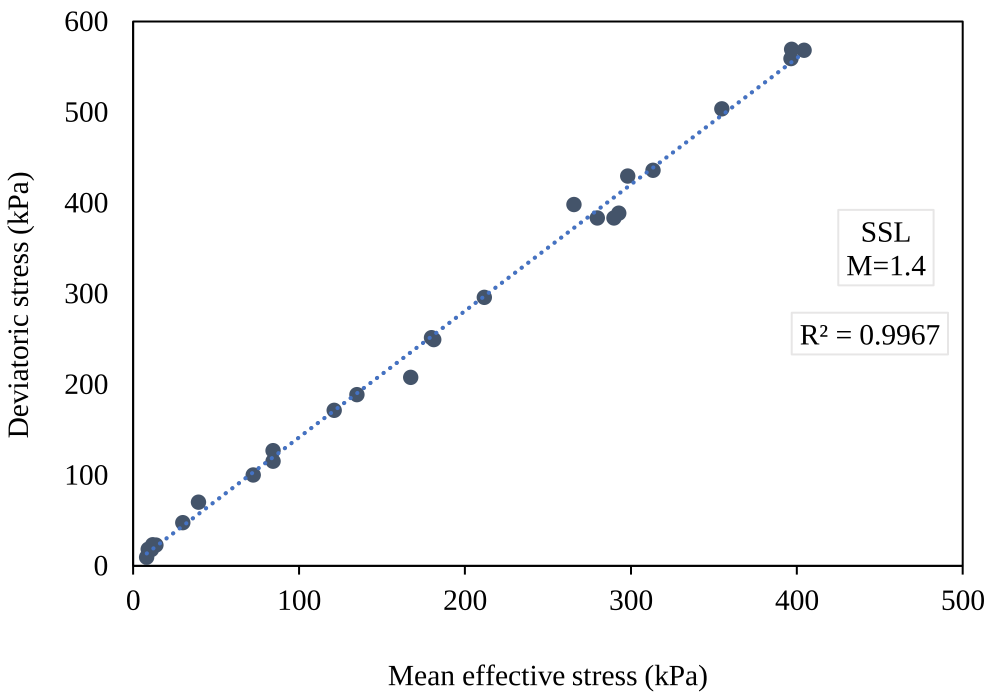

Figure 6. Steady state line in q-p′ plane.

3.1. Effect of confining pressure on sand behavior

In this study, sand behavior was controlled by the relative density and confining pressure, which, respectively, decrease and increase the liquefaction potential. Confining pressure is a parameter that relates to the depth and surcharge. Figure 7 displays the effective stress paths at different effective confining pressure at isotropic and anisotropic stress conditions for initial relative density of the sand, D_{r0} = 45%. It can be observed that on increasing the effective confining pressure, the stress path tends to reach steady state, whereby there is a change in its direction indicating liquefaction. As stated by Rezaian et al. [27], the increase in confinement results in increase of particle breakage therefore since the particles are brittle means more breakage of particles and this leads to reach to the critical state and resulting in liquefaction.

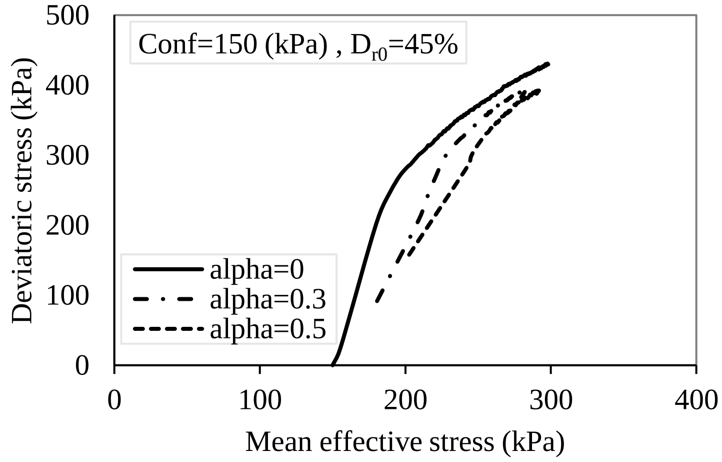

(**a**)

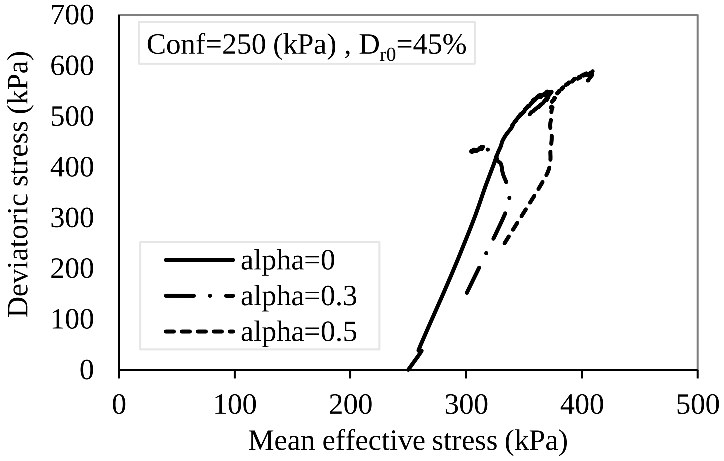

(**b**)

Preprints (www.preprints.org) | NOT PEER-REVIEWED | Posted: 5 September 2020 doi:10.20944/preprints202009.0118.v1

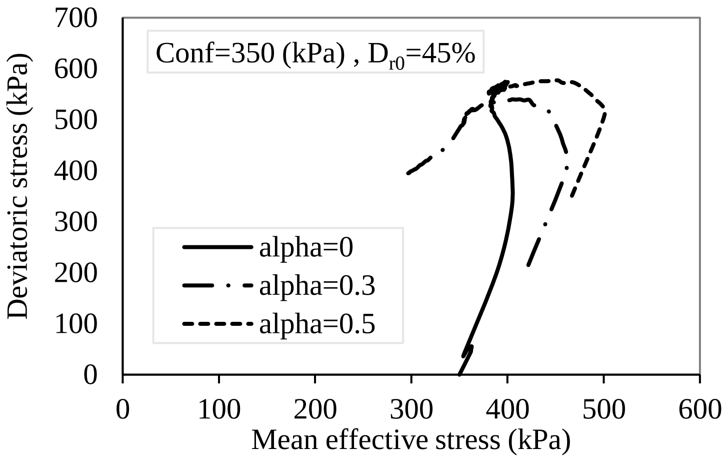

(c)

Figure 7. Effective stress paths at different effective confining pressure a) 159 kPa, b) 250 kPa, c) 350 kPa in isotropic and anisotropic stress condition for D_{r0}= 45%

3.2. Initial shear stress ratio (α)

The initial shear load parameter α obtained by anisotropically consolidating the specimens can differ according to certain soil parameters. Compared to level ground conditions (α = 0), only a few experimental studies on the monotonic behavior of sands in sloping ground conditions (α > 0) are available, where the shear component is also present during the initial static condition. Therefore, this study (18 tests) includes anisotropically consolidated specimens prepared with initial axial loading in a drained condition. The initial shear stress ratio α is defined as the ratio of the initial axial stress (q_s) divided by twice the effective confining stress (σ_{3c}).

For example, when α=0.5 and σ_{3c}=150 kPa, the load will be 0.29 kN, and for σ_{3c}= 250 kPa, the specimens will undergo a 0.49-kN load. Equation (1) indicates that the initial static shear stress level increases with the increase in α values, and the limiting case of α=0 represents level ground conditions without the initial static shear stress. Depending on the density of soil and the initial effective stress level, the presence of initial static shear stress may have either have an improving or aggravating impact on the resistance to liquefaction.

$$\alpha = \frac{\tau}{\sigma'_{3c}} = \frac{q_s}{2\sigma'_{3c}} = \frac{\grave{\sigma}_{1c}-\grave{\sigma}_{3c}}{\grave{\sigma}_{1c}+\grave{\sigma}_{3c}}, \quad (1)$$

The excess pore water pressure (PWP) buildup of three specimens with a relative density of 45%, confining pressure of 150 kPa, and different initial shear stress (α=0, 0.3, and 0.5) are shown in Figure 8. All the samples in these three tests exhibit dilative behaviors because of the high relative densities, whereas their PWP intensities differ depending on the initial shear stress ratio. In addition, on increasing the initial shear stress, the PWP peak declines and subsequently, the intensity of dilation increases. Due to the reduction in the excess pore pressure, the particle contact friction increases and causes resistance to liquefaction.

Preprints (www.preprints.org) | NOT PEER-REVIEWED | Posted: 5 September 2020 doi:10.20944/preprints202009.0118.v1

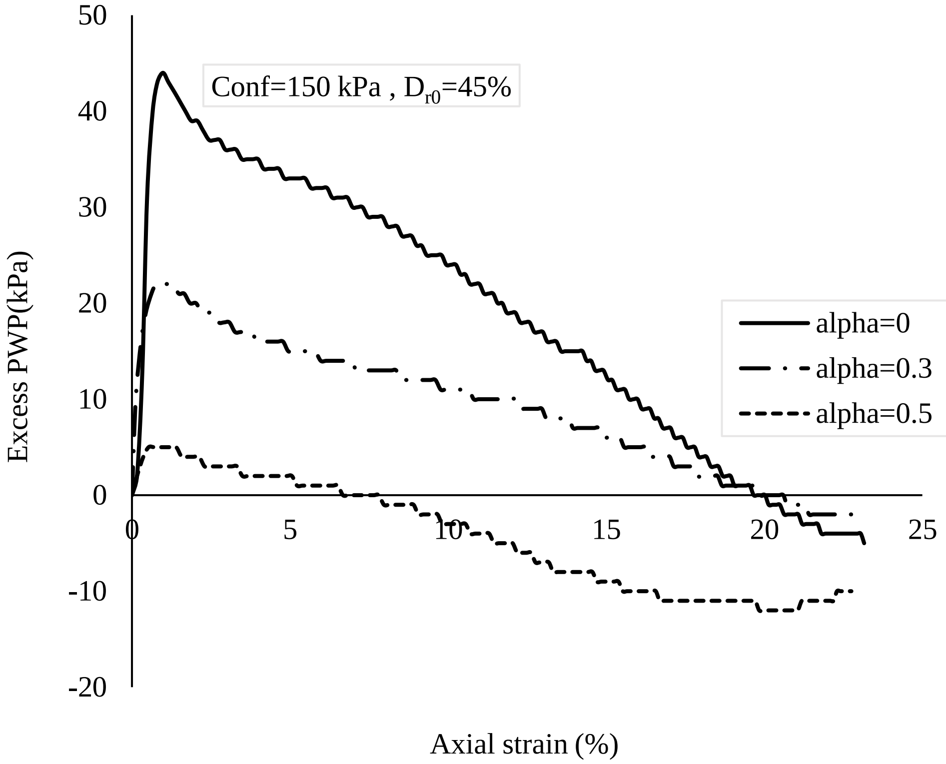

Figure 8. Comparative curvature for $(R\text{-}A)_3$, $(R\text{-}B)_3$ and $(R\text{-}C)_3$ in u-ε% plane.

Figure 9 displays different initial shear stress with higher confinement (250 kPa) compared to Figure 8. It can be seen that the initial shear stress not only changes the behavior intensity, but also the entire behavior to dilation in $(R\text{-}A)_6$, liquefaction in $(R\text{-}B)_6$ and limited liquefaction in $(R\text{-}C)_6$, where the initial shear stress ratios are 0, 0.3, and 0.5, respectively. This result is completely different from those observed in the specimens in Figure 8, where the excess PWP buildup is considerably more and has be preserved up to high strain levels. The increase in PWP reduces the effective stress, which is the particle skeleton strength (reduction in the particle contact friction); therefore, such reduction leads to liquefaction. This may also show the inverse dependency of α on the effective confining pressure.

 doi:10.20944/preprints202009.0118.v1

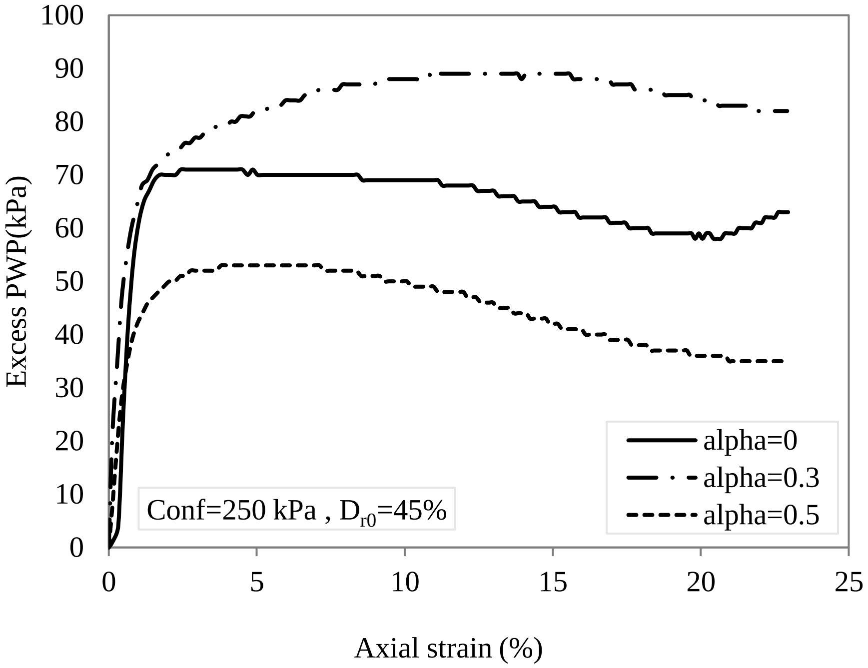

Figure 9. comparative curvatures for (R-A)$_6$, (R-B)$_6$ and (R-C)$_6$ in u-ε% plane.

3.3. Pore water pressure ratio (r_u)

The observations in Figures 8 and 9 regarding the effect of confinement on the excess pore pressure, on varying the initial shear stress ratios, can be a criterion for liquefaction susceptibility. From equation 2, it can be observed that the criterion for liquefaction susceptibility pore water pressure ratio (ru) is the variation of the pore water pressure at failure to the initial effective confining pressure.

$$r_u = \frac{u_{excess\ at\ failure}}{\sigma'_{3c}}, \tag{2}$$

The susceptibility ranges from 0–1, when r_u approximates unity, and the liquefaction potential increases. Jafarian et al. [5] had also stated that it is common to have lower r_u within the liquefaction phenomenon, termed as susceptible to liquefaction. Figure 10 presents the liquefaction susceptibility for isotropic and anisotropic specimens; the pore water pressure ratio (r_u) is plotted against the mean effective pressure at failure (Figure10). It can be seen that most specimens are susceptible to liquefaction, while three of them show a negative value indicating that they have no liquefaction potential. In this study, the r_u values range from -0.06–0.97. However, 21 out of the 24 tests show a positive value of r_u indicating liquefaction behavior.

Preprints (www.preprints.org) | NOT PEER-REVIEWED | Posted: 5 September 2020 doi:10.20944/preprints202009.0118.v1

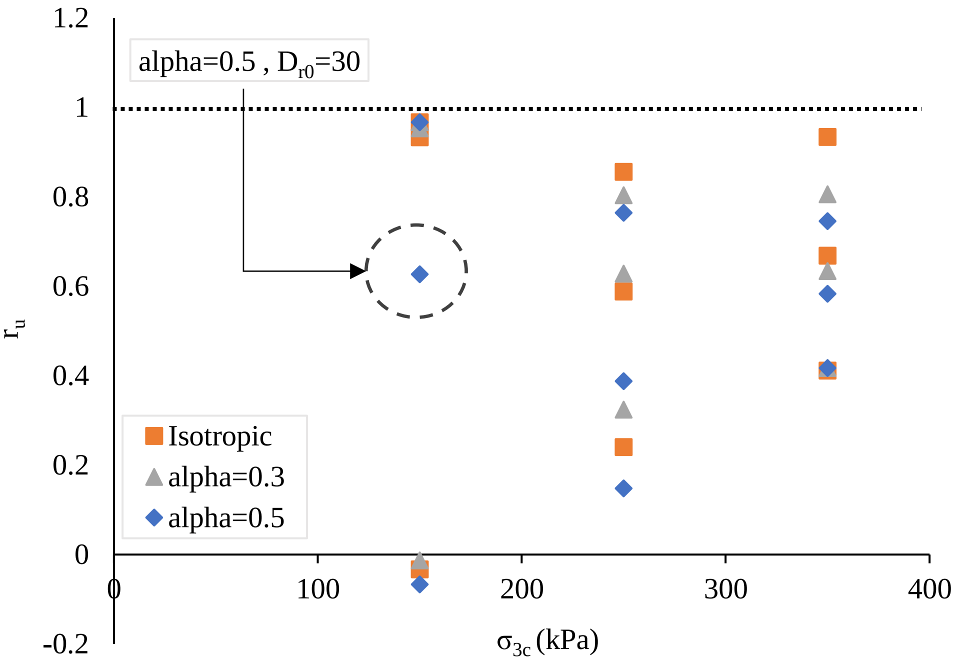

Figure 10. Pore water pressure ratio versus mean effective stress and effective confining pressure in isotropic and anisotropic stress condition.

In Figure 10, the scattered pattern of points shows that r_u is related to the relative density (D_r) because on increasing the effective confining pressure from 150 kPa to 350 kPa, the dispersion decreases. The dispersion in tests with σ_{3c} = 150 kPa reveals that except for one of the tests $(R-C)_2$, which may be an outlier, the outcomes of the other tests fall into two main opposing groups (phases): 1-highly susceptible and 2- completely nonsusceptible to liquefaction.

As observed from the r_u values plotted against the initial relative densities and from the point dispersion comparison shown in Figure 11, specimens with low D_{r0} exhibit almost the same behavior, whereas for those with high D_{r0}, the tests results differ to a certain extent from each other. For medium D_{r0}, two distinguishable points, $(R-A)_2$ and $(R-B)_2$, indicate the commencement of dispersion. It is clear from Figure 11 that the increase in relative density reduces the liquefaction susceptibility. As stated by Zhao et al. [31], specimens with high relative density have lower particle failure probability and less extensive failure modes than loose specimens. Additionally, loose specimens exhibit higher compression due to particle failure leading to more fine generation by the further crushing of existing fragments, and as stated earlier, reach the critical state, resulting in liquefaction.

Preprints (www.preprints.org) | NOT PEER-REVIEWED | Posted: 5 September 2020 doi:10.20944/preprints202009.0118.v1

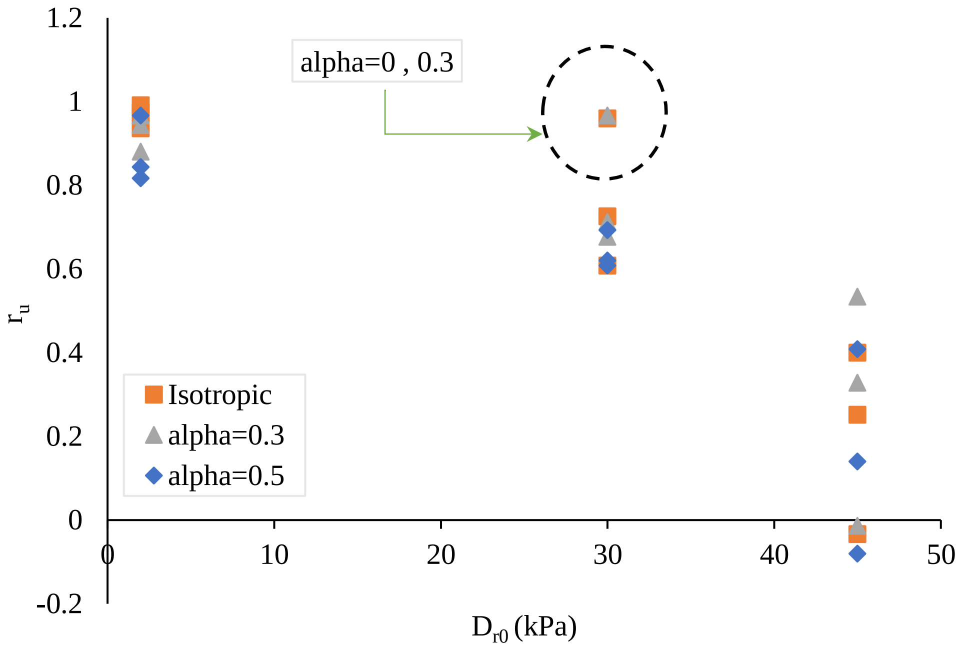

Figure 11. Pore water pressure ratio versus mean effective stress and effective confining pressure in isotropic and anisotropic stress conditions.

The friction angle at the failure point and r_u have a negative correlation, as depicted in Figure 12. The friction angle ranges from 2–36 in this study, and $\phi'_{(deg)} = 2$ and $\phi'_{(deg)} = 36$ are related to specimens with high and low susceptibility to liquefaction, respectively. Low friction angle is a result of excess pore water pressure, causing loss of contact between particles which in turn results in interparticle friction loss.

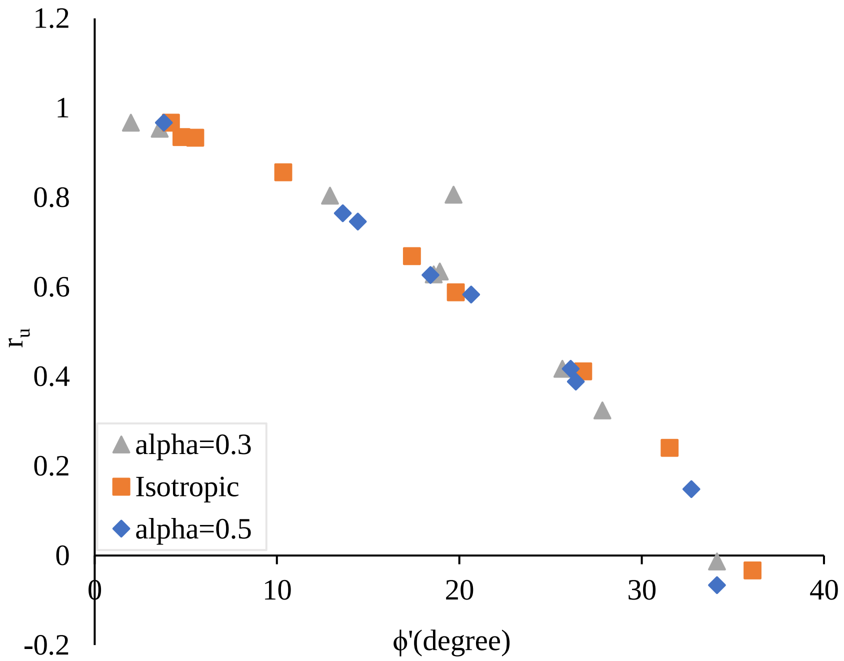

Figure 12. Pore water pressure ratio versus friction angle at failure in isotropic and anisotropic stress.

Preprints (www.preprints.org) | NOT PEER-REVIEWED | Posted: 5 September 2020 doi:10.20944/preprints202009.0118.v1

3.4. Pore water pressure ratio versus the initial shear stress ratio

Figure 13 displays the relationship between r_u and α in three charts, whose effective confining pressures are different. It is obvious from the charts that on increasing the relative density, the liquefaction susceptibility reduces regardless of whether α and σ_{3c} increase or decrease. This indicates that the relative density is much more effective than α and σ3c. Figure 13(a) shows that the initial shear stress is not effective in loose sand (2%), whereas it influences semi-dense and dense specimens. In Figure 13(b), this pattern slightly changes because the relative density after consolidation increases, which is strongly related to the effective confining pressure for loose sand. For example, as shown in Table 2, the relative density increases from 2% to approximately 23% after consolidation in sample $(R\text{-}A)_7$, whereas this growth is approximately 12% in sample $(R\text{-}A)_1$. This increment was calculated using the amount of water raised up during volume change in the consolidation process. The specimen became denser due to the increase in σ_{3c} from 150 to 250 kPa, and this pattern continued, when the effective confining pressure was increased from 250 to 350 kPa (Figure 13(c)). For the other relative densities, except for specimens with σ_{3c} = 350 kPa, all the functions initially increased to α=0.3 and then decreased to α=0.5 which can indicate a lesser decreasing effect for higher values of α than for the medium values, for susceptibility under medium effective confining pressure. This phenomenon is also shown in Figure 10 by the change in test result from liquefaction to quasi-limited liquefaction, when α is increased from 0.3 to 0.5. In Figure 13(c), when σ_{3c} = 350 kPa, the pattern remains unchanged for α>0. Moreover, the functions hardly change.

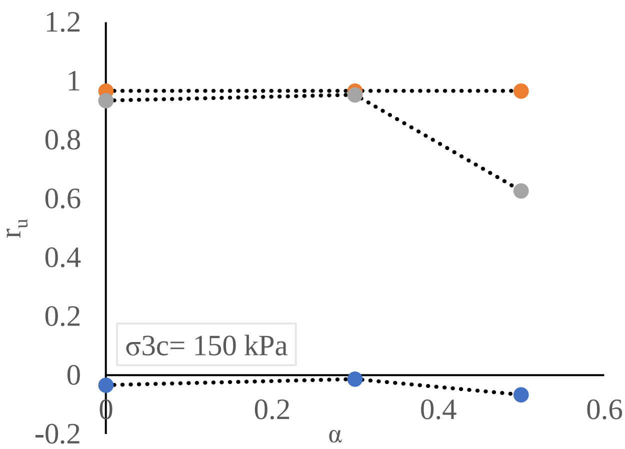

(**a**)

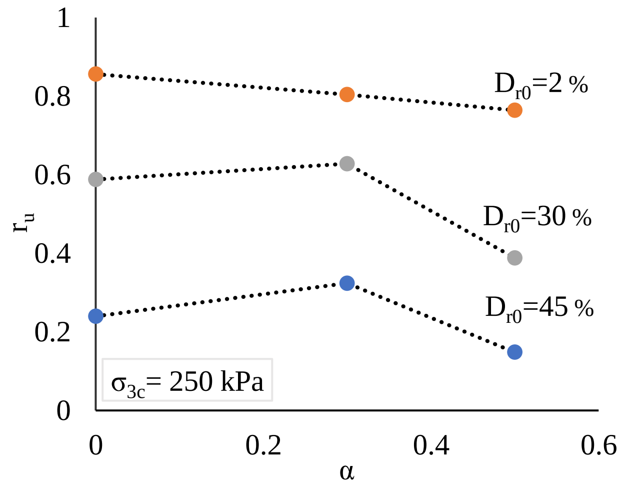

(**b**)

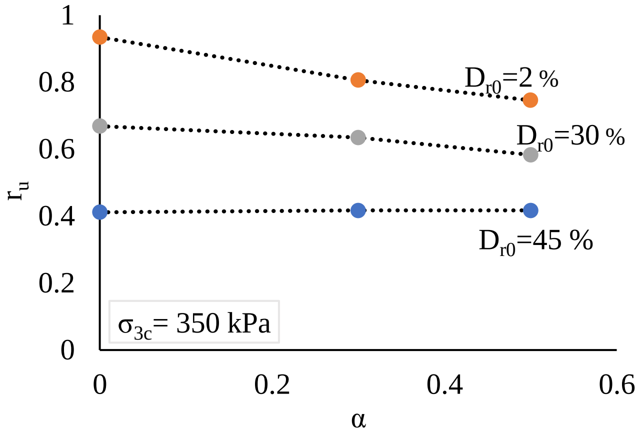

(c)

Figure 13. Pore water pressure ratio versus initial shear stress ratio at a) 159 kPa, b) 250 kPa and c) 350 kPa effective confining pressure.

4. Conclusions

In this study, 27 isotropic and anisotropic monotonic undrained triaxial tests were performed to investigate the liquefaction susceptibility in relation to the critical state soil mechanics and micromechanical behavior. It was observed that Ramsar sand can experience all the possible behaviors of liquefiable soils, namely, flow failure, limited liquefaction, and dilation. In addition, Ramsar sand is highly susceptible to liquefaction because 21 out of the 27 tests showed flow liquefaction. Among the other six tests, two showed limited liquefaction and only four showed dilation. Another important result was that the grains of Ramsar sand are brittle, which is responsible for its high susceptibility to liquefaction because a crushed specimen becomes more resistant to liquefaction (q_u-before = 255.9 kPa and q_u-after = 283.85 kPa). The initial shear stress α is a critical parameter for studying soil behavior on a slope and/or under a structure. Although it has limited impact on loose sand, it can be an improving or aggravating factor depending on the effective confining pressure and relative density levels. The liquefaction susceptibility increased for an α range of 0–0.3 and reduced for a range of 0.3–0.5 under medium effective confining pressure and lower. However, at high effective confining pressure, r_u values barely reduces as a result of increasing the initial shear stress ratio.

The pore water pressure ratio r_u is a key parameter for evaluating sand behavior. In the conducted tests, even though only six tests did not result in liquefaction, only three of them showed negative r_u values. For the other three tests with positive values of r_u, the susceptibility to liquefaction despite showing dilation or limited liquefaction is not surprising. Furthermore, a similar study is recommended to evaluate the findings of this study by investigating the varying particle minerology and percentage of fine generation due to particle breakage after shearing at various testing conditions.

Author Contributions: MN and SS conceived the study and were responsible for the scheduling and performing the experimental study. AE was responsible for structure interpretation. SS and AI wrote the first draft of the article and AE overlooked and finalized the study.

Funding: This research received no external funding.

Acknowledgments: The authors appreciate Kavosh Khak Azma Co. for providing triaxial apparatus and other laboratory equipment to conduct this study.

Conflicts of Interest: The authors declare no conflict of interest.

References

1. Marcuson, W.F. DEFINITION OF TERMS RELATED TO LIQUEFACTION. *ASCE J Geotech Eng Div,* **1978**.
2. Youd, T.L.; Idriss, I.M.; Andrus, R.D.; Arango, I.; Castro, G.; Christian, J.T.; Dobry, R.; Finn, W.D.L.; Harder, L.F.; Hynes, M.E.; et al. Liquefaction resistance of soils: Summary report from the 1996 NCEER and 1998 NCEER/NSF workshops on evaluation of liquefaction resistance of soils. *J. Geotech. Geoenvironmental Eng.* **2001**.
3. Castro, G. Liquefaction of sands. *Harvard Soil Mech. Ser. 87, Harvard Univ. Cambridge, Massachusetts.* **1969**.
4. Poulos, S.J.; Castro, G.; France, J.W. Liquefaction evaluation procedure. *J. Geotech. Eng.* **1985**.
5. Jafarian, Y.; Ghorbani, A.; Salamatpoor, S. Experimental study on shear resistance of Babolsar sand under anisotropic consolidation. *3rd Int. Conf. New Dev. Soil Mech. Geotech. Eng. Cyprus.* **2012**.
6. Been, K.; Jefferies, M.G. A state parameter for sands. *Geotechnique* **1985**.
7. Vaid, Y.P.; Chung, E.K.F.; Kuerbis, R.H. Stress path and steady state. *Can. Geotech. J.* **1990**.
8. Lade, P. V. Static instability and liquefaction of loose fine sandy slopes. *J. Geotech. Eng.* **1992**.
9. Ishihara, K. Liquefaction and flow failure during earthquakes. *Geotechnique* **1993**.
10. Wanatowski, D.; Chu, J. Static liquefaction of sand in plane strain. *Can. Geotech. J.* **2007**.
11. Bobei, D.C.; Lo, S.R. Static liquefaction of Sydney sand mixed with both plastic and non-plastic fines. *Proc. 14th Southeast Asian Geotech. Conf. Hong Kong* **2001**, 9–14.
12. Ekinci, A.; Hanafi, M.; Ferreira, P.M.V. Influence of Initial Void Ratio on Critical State Behaviour of Poorly Graded Fine Sands. *Indian Geotech. J.* **2020**.
13. Kramer, S.L.; Seed, H.B. Initiation of soil liquefaction under static loading conditions. *J. Geotech. Eng.* **1988**.
14. Harder, L.F.J.; Boulanger, R.W. Application of K_ and KA correction factors. *Proc. NCEER Work. Eval. Liq. Resist. soils, Natl. Cent. Earthq. Eng. Res. State Univ. New York Buffalo* **1997**, 176–190.
15. Seed, R.B.; Harder, Leslie F., J. SPT-Based Analysis of Cyclic Pore Pressure Generation and Undrained Residual Strength. In Proceedings of the H. Bolton Seed Memorial Symposium; **1990**.
16. Yang, J.; Sze, H.Y. Cyclic behaviour and resistance of saturated sand under non-symmetrical loading conditions. *Geotechnique* **2011**.
17. Wei, X.; Yang, J. The effects of initial static shear stress on liquefaction resistance of silty sand. *6th Int. Conf. Earthq. Geotech. Eng. 1-4 November, Christchurch, New Zealand.* **2015**.
18. Castro, G.; Poulos, S.J. FACTORS AFFECTING LIQUEFACTION AND CYCLIC MOBILITY. *ASCE J Geotech Eng Div* **1977**.
19. Roscoe, K.H.; Schofield, A.N.; Wroth, C.P. On The Yielding of Soils. *Géotechnique* **1958**, *8*, 22–53.
20. Schofield, A.; Wroth, P. Critical state soil mechanics. *McGraw-hill* **1968**.
21. Wroth, C.P.; Bassett, R.H. A stress-strain relationship for the shearing behaviour of a sand. *Geotechnique* **1965**.
22. Roscoe, K.H. The influence of strains in soil mechanics. *Geotechnique* **1970**.
23. Been, K.; Hachey, J.; Jefferies, M.G. The critical state of sands. *Geotechnique* **1991**.
24. Coop, M.R. The mechanics of uncemented carbonate sands. *Géotechnique* **1990**, *40*, 607–626.
25. Ferreira, P.M. V.; Bica, A.V.D. Problems in identifying the effects of structure and critical state in a soil with a transitional behaviour. *Géotechnique* **2006**, *7*, 445–454.
26. Coop, M.R. On the mechanics of reconstituted and natural sands. In Proceedings of the Deformation Characteristics of Geomaterials : Recent Investigations and Prospects - International Symposium on

Preprints (www.preprints.org) | NOT PEER-REVIEWED | Posted: 5 September 2020 doi:10.20944/preprints202009.0118.v1

Deformation Characteristics of Geomaterials, ISLyon 2003; 2005.
27. Rezaeian, M.; Ferreira, P.M.V.; Ekinci, A. Mechanical behaviour of a compacted well-graded granular material with and without cement. *Soils Found.* **2019**.
28. Cavarretta, I.; Coop, M.; O'Sullivan, C. The influence of particle characteristics on the behaviour of coarse grained soils. *Geotechnique* **2010**.
29. Senetakis, K.; Coop, M.R.; Todisco, M.C. The inter-particle coefficient of friction at the contacts of Leighton Buzzard sand quartz minerals. *Soils Found.* **2013**.
30. Zhang, X.; Baudet, B.A.; Yao, T. The influence of particle shape and mineralogy on the particle strength, breakage and compressibility. *Int. J. Geo-Engineering* **2020**.
31. Zhao, B.; Wang, J.; Andò, E.; Viggiani, G.; Coop, M.R. Investigation of particle breakage under one-dimensional compression of sand using x-ray microtomography. *Can. Geotech. J.* **2020**.
32. McDowell, G.R.; Bolton, M.D. On the micromechanics of crushable aggregates. *Geotechnique* **1998**.
33. Coop, M.R.; Sorensen, K.K.; Freitas, T.B.; Georgoutsos, G. Particle breakage during shearing of a carbonate sand. *Geotechnique* **2004**.
34. Chandler, H.W. A plasticity theory without drucker's postulate, suitable for granular materials. *J. Mech. Phys. Solids* **1985**.
35. Jefferies, M.; Been, K. Liquefaction: A Critical State Approach. *CRC Press* **2006**.
36. Kramer, S.L. *Geotechnical Earthquake Engineering*; **1996**;
37. ASTM D4253-2016, Standard Test Methods for Maximum Index Density and Unit Weight of Soils Using a Vibratory Table. *ASTM Int. West Conshohocken, PA.* **2016**.
38. ASTM D4254 - 16, Standard Test Methods for Minimum Index Density and Unit Weight of Soils and Calculation of Relative Density. *ASTM Int. West Conshohocken, PA.* **2016**.
39. Lade, P. V.; Duncan, J.M. CUBICAL TRIAXIAL TESTS ON COHESIONLESS SOIL. *ASCE J Soil Mech Found Div* **1973**.
40. Ventouras, K. Engineering behaviour of thanet sand, Imperial College of Science, Technology & Medicine, **2005**.
41. Cheng, Z.; Wang, J.; Coop, M.R.; Ye, G. A miniature triaxial apparatus for investigating the micromechanics of granular soils with in situ X-ray micro-tomography scanning. *Front. Struct. Civ. Eng.* **2020**.